ISSN (Print) 1226-1750
ISSN (Online) 2233-6656
Journal of Magnetics 29(1), 117-122 (2024) https://doi.org/10.4283/JMAG.2024.29.1.117

Fusion Algorithm in Magnetic Resonance/Positron Emission Tomography using Attenuation Correction based on Ultrashort Echo-Time Pulse Sequences

Chanrok Park[1] and Youngjin Lee[2]*

[1]*Department of Radiological Science, Eulji University, 553, Sanseong-daero, Sujeong-gu, Seongnam-si, Gyeonggi-do, Republic of Korea*
[2]*Department of Radiological Science, Gachon University, 191, Hambakmoero, Yeonsu-gu, Incheon, Republic of Korea*

(Received 14 September 2023, Received in final form 12 December 2023, Accepted 8 February 2024)

Positron emission tomography (PET) images in magnetic resonance (MR)/PET fusion imaging systems are corrected for parts attenuated by gamma-rays by various MR pulse sequences. We aimed to study the quality of MR/PET images using an attenuation correction method based on ultrashort echo-time (UTE) pulse sequences. The proposed image-quality improvement algorithm was modeled as a convergence of the median-modified Wiener filter (MMWF) for noise reduction and Prewitt operator for emphasizing the edge area. By applying the proposed algorithm to MR/PET images, superior contrast to noise ratio and coefficient of variation values were obtained compared to those in the original image. The edge rise distance data of the proposed algorithm exhibited a very small difference from that of the original MR/PET image (difference: 2.21 %). In conclusion, we confirmed the applicability and usefulness of MMWF and Prewitt operator in UTE-based MR/PET imaging.

Keywords: magnetic resonance/positron emission tomography fusion image, ultrashort echo-time pulse sequence, convergence algorithm using median-modified Wiener filter and prewitt operator, evaluation of image quality

1. Introduction

Recently, anatomical and functional fusion imaging has attracted significant attention in diagnostic medicine [1]. Magnetic resonance (MR)/positron emission tomography (PET) was first proposed in the 1990s [2], and began to develop rapidly with the development of detector modules and systems capable of acquiring PET images even in magnetic fields [3]. Recently, integrated MR/PET systems have also been used in preclinical and clinical fields, contributing to the accurate diagnosis of Alzheimer's and cardiovascular diseases [4, 5]. The MR/PET system has the advantage of being able to accurately quantify the sensitivity of various stages of Alzheimer's disease and reducing motion artifact when imaging cardiovascular disease.

The basic principle of PET is the detection of gamma rays emitted from radioisotope [6, 7]. Since only one of the two gamma rays generated from a radioisotope is lost, it is assumed to be attenuated; therefore, an attenuation correction process must be performed during the PET image acquisition process [8]. In whole-body ^{18}F- Fluorodeoxyglucose (FDG) PET images, when attenuation correction is not performed, a pattern different from the actual distribution of glucose metabolism in the human body is observed; therefore, caution is required [9].

CT images based on X-rays are primarily used for attenuation correction of PET images [10, 11]. However, to be used appropriately in MR/PET systems, algorithms that can be used for the attenuation correction of MR images are required, and several relevant studies have been actively conducted. In the early stages of research, methods using brain MR image segmentation and standard templates were used, and various pulse sequences have been developed and applied for the attenuation correction of PET images [12, 13]. Among the various pulse sequences, ultrashort echo-time (UTE), which can be approximately 10-20 times shorter than the echo-time (TE) sequence mainly used in clinical practice, has been recognized as an attenuation correction method [14]. As this sequence is not modeled based on anatomical reference data, it has the advantage of being able to distinguish all the attenu-

*Corresponding author: Tel: +82-32-820-4362
Fax: +82-32-820-4449, e-mail: yj20@gachon.ac.kr

ation information [15]. Keereman *et al*. analyzed its applicability to various tissues using the relaxation time derived from MR images acquired using a UTE pulse sequence [16]. The final quality of the PET image with attenuation correction based on this UTE pulse sequence is inevitably lower than that of the gold standard image. Noise and spatial resolution are representative PET image quality evaluation parameters, and it is important to develop methods that can maximally improve these two parameters. Image filtering is widely used as the most efficient and simple method to reduce noise in functional images [17-19]. Among the filtering methods, the usefulness of the median-modified Wiener filter (MMWF), which combines the advantages of the median and Wiener filters, in functional images was proven by Park *et al*. [17].

However, the deteriorated edge information-preservation ability of PET images resulting from filtering methods, including MMWF, requires further improvement. The Prewitt operator is a representative image edge information improvement approach that has proven to be superior to the Canny edge method in preserving the edges of photon-based images [20] and has been applied in various ways to medical images [21]. Thus, the purpose of this study was to analyze the applicability of an algorithm that combines the MMWF and Prewitt operators for attenuation-corrected MR/PET images using UTE pulse sequences.

2. Materials and Methods

A flow chart showing the overall research flow is shown in Fig. 1. The final result image was derived by applying a fusion algorithm combining MMWF and Prewitt operator to the acquired MR/PET images.

2.1. MR/PET system and phantom

The MR/PET system used in this study was a 3.0 T-based Biograph mMR scanner (Siemens Healthineers, Erlangen, Germany). The MR/PET image acquisition parameters using the UTE pulse sequence were: repetition time (TR) 11.94 ms and TE 0.07 ms. In addition, the field of view of the image was set to 300 mm^2 and a matrix size of 192 × 192 was applied. Jaszczak phantom (Data Spectrum, Chapel Hill, NC, USA) images consisting of holes with different diameters (15.9, 19.1, 25.4, and 31.8 mm) were acquired. NaCl and ^{18}F radioisotopes were injected into each sphere; a schematic diagram is shown in Fig. 2.

2.2. Fusion algorithm modeling combining MMWF and Prewitt operator

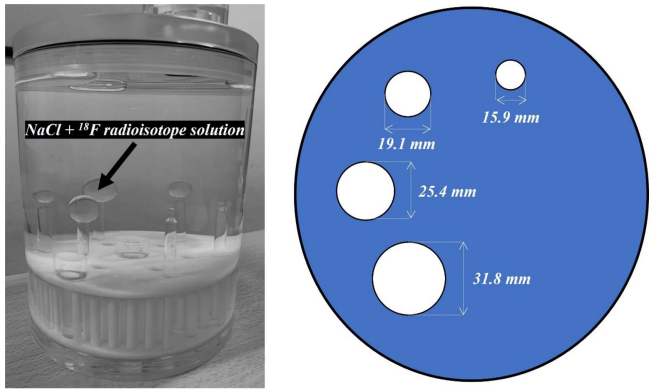

Fig. 2. (Color online) Illustration of the experimental setup: (a) photograph of the phantom containing a mixed solution of NaCl and ^{18}F radioisotope used in the actual study and (b) schematic diagram (top view) of the phantom with the indicated hole diameter.

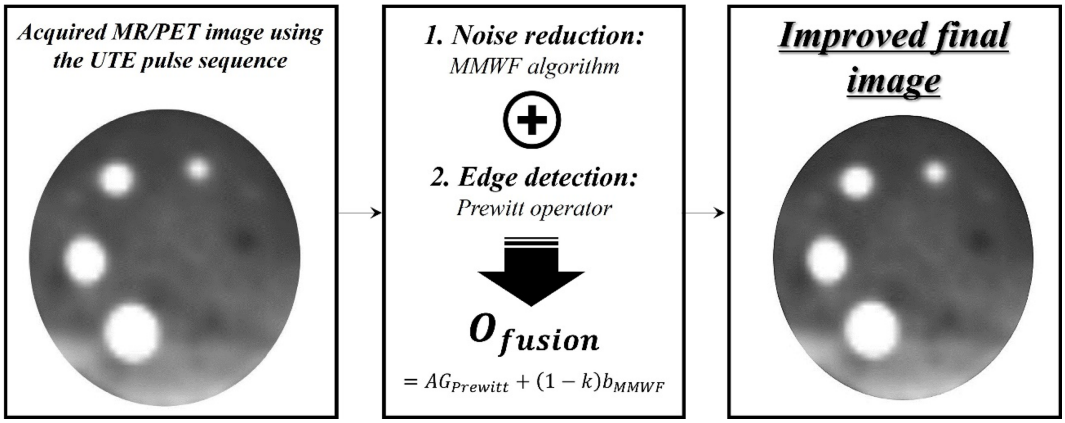

Fig. 1. Schematic diagram of the entire research flow. The final result image was obtained by applying the fusion algorithm to the MR/PET image acquired using the UTE pulse sequence.

MMWF used for removing noise from MR/PET images was modeled based on the method proposed by Cannistraci *et al*. [22]. MMWF is a nonlinear adaptive filter that combines median and Wiener filters to improve the noise reduction efficiency and image edge-information preservation. The formula for MMWF ($b_{mmwf}(x, y)$) is as follows:

$$b_{mmwf}(x,y) = \tilde{\mu} + \frac{\sigma^2 - v^2}{\sigma^2}[a(x,y) - \tilde{\mu}] \quad \left(\tilde{\mu} = \frac{1}{NM}\sum_{n,m\epsilon\eta} a(x,y)\right) \tag{1}$$

where $\tilde{\mu}$ is the median values around pixel (N-by-M size area); σ^2 and v^2 are the variance in the Gaussian noise and the variance of noise of the Wiener filter, respectively; and $a(x, y)$ is the pixel value at (x, y) position. In this study, the mask size of MMWF was set to the default value for modeling.

The principles of applying weights to adjacent pixels and convolving masks in the horizontal, vertical, and diagonal directions are widely used to detect the edges of an image. The edge detection method using the Prewitt operator applies gradient masks in the horizontal and vertical directions in the spatial domain [23].

Lee modeled an algorithm that combines the noise reduction and edge detection methods [20]. Based on the aforementioned references, an image quality improvement algorithm that combines MMWF and Prewitt operators was modeled as follows:

$$O_{fusion} = AG_{Prewitt} + (1-k)b_{MMWF} \tag{2}$$

where O_{fusion} is the final image obtained using the fusion algorithm, A is the original image, $G_{Prewitt}$ is the edge operation of the Prewitt method, and k is a constant.

2.3. Quantitative evaluation of image quality

The contrast to noise ratio (CNR) and coefficient of variation (COV) were calculated to evaluate the noise levels in the acquired MR/PET images. The formulae for the two evaluation parameters are as follows [24, 25]:

$$CNR = \frac{|S_{target} - S_{background}|}{\sqrt{\sigma_{target}{}^2 + \sigma_{background}{}^2}} \tag{3}$$

$$COV = \frac{\sigma_{target}}{S_{target}} \tag{4}$$

where S_{target} and σ_{target} denote the intensity and standard deviation in the target area, respectively; and $S_{background}$ and $\sigma_{background}$ denote the intensity and standard deviation in the background area, respectively. In addition, the edge rise distance (ERD) evaluation parameter was used to measure the degree of edge preservation. The region of interest (ROI) for calculating CNR, COV, and ERD is shown in Fig. 3. The CNR and COV values were averaged by setting ROIs in the three areas, and the ERD values were analyzed by setting a profile line.

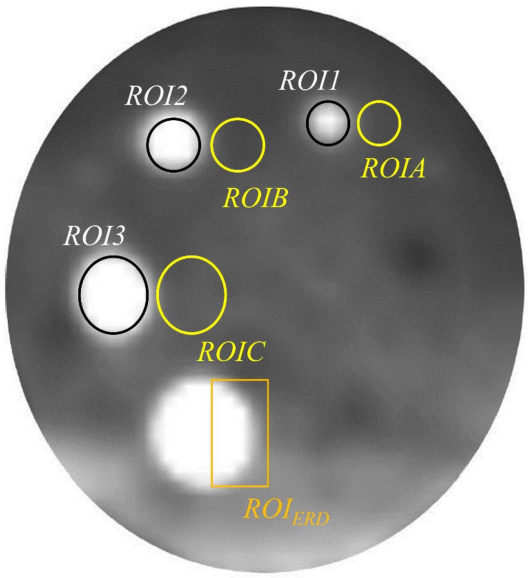

Fig. 3. (Color online) Region of interest (ROI) schematic diagram for quantitative evaluation of magnetic resonance (MR)/positron emission tomography (PET) images. The target and background areas for contrast-to-noise ratio (CNR) and coefficient of variation (COV) evaluation were marked from ROI1 to ROI3 and ROIA to ROIC, respectively.

3. Results and Discussion

Fig. 4 shows the resulting MR/PET images, including those obtained using the proposed algorithm. Fig. 5 shows a magnified image of the smallest hole in the Jaszczak phantom. When MMWF and the algorithm combining MMWF and Prewitt operators were applied to the MR/PET images, we visually confirmed that the noise level was reduced compared to the original image. In the image to which an algorithm combining MMWF and the Prewitt operator was applied in the original image, the edge area was clearly observed compared to the image to which only MMWF was applied. When only MMWF was applied to the image, we were able to observe parts where the edge became ambiguous (red arrow in Fig. 5(b)), whereas in the image to which the proposed algorithm was applied, the edge was observed to be similar to that of the original image (blue arrow in Fig. 5(a)). In addition, when using the proposed algorithm, the contrast improved during the application of the Prewitt operator, resulting in an overall brighter image.

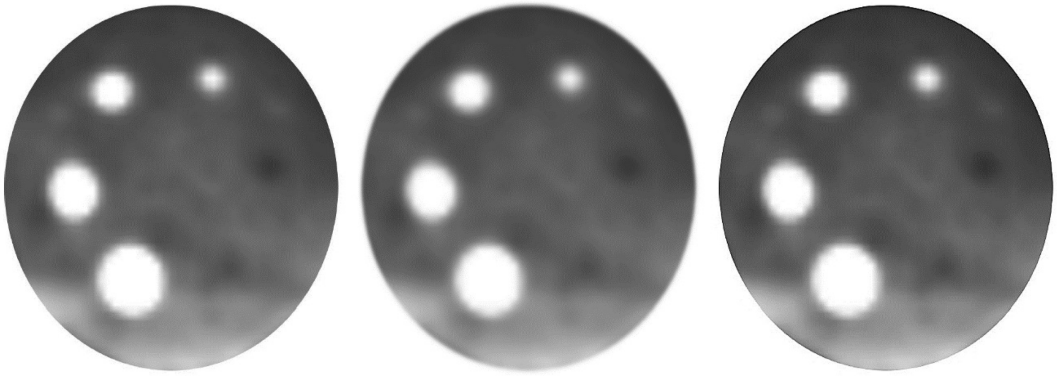

Fig. 4. Magnetic resonance (MR)/positron emission tomography (PET) result image: (a) original image, (b) the median-modified Wiener filter (MMWF) noise reduction method, and (c) algorithm combining MMWF and the Prewitt operator.

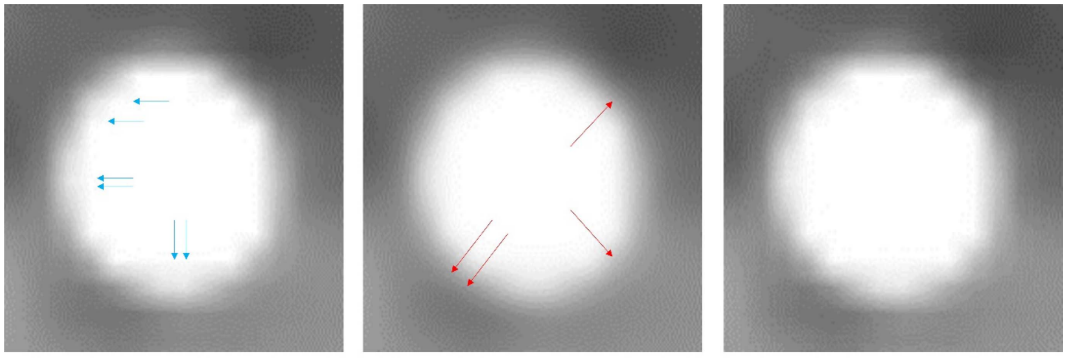

Fig. 5. Magnetic resonance (MR)/positron emission tomography (PET) image enlarging the 15.9-mm diameter area of the used phantom. The edge areas observed in the original image (blue arrow) were blurred in the image (b) where only the median-modified Wiener filter (MMWF) noise reduction method was applied, and when the proposed algorithm (c) was used, an edge area similar to (a) was observed.

Figs. 6(a), (b), and (c) show graphs of the quantitative evaluation results of CNR, COV, and ERD in the acquired images, respectively. As shown in Fig. 6(a), the best CNR results were obtained using the proposed algorithm (Fig. 6(a)). The average CNR values in the three ROIs were 22.43, 28.42, and 28.91 for the original image, MMWF, and algorithm combining MMWF and Prewitt operator, respectively. We confirmed that the CNR value in the MR/PET images using the proposed algorithm improved by approximately 28.89 % compared to the original image. The rate of noise reduction was similar when only MMWF was used, and when the proposed algorithm was applied to the image, we believe that the difference in image quality improvement ability between the two methods occurred in the contrast area.

Superb COV results were obtained when only MMWF was applied to the acquired images (Fig. 6(b)). The average COV values in the three ROIs were 0.727, 0.665, and 0.670 for the original image, MMWF, and the algorithm combining MMWF and the Prewitt operator, respectively. We confirmed that the COV value in the MR/PET images using the proposed algorithm improved by approximately 7.89 % compared to the original image. The COV difference between the images obtained using the proposed algorithm and MMWF was confirmed to be very small (0.64 %).

For the ERD results, the best value was obtained in the original image, and the lowest value was obtained with MMWF (Fig. 6(c)). The ERD values using profile line were 6.34, 7.63, and 6.48 for the original image, MMWF, and the algorithm combining MMWF and the Prewitt operator, respectively. The ERD results obtained by applying the proposed algorithm to MR/PET images showed differences of approximately 2.21 % and 15.07 %

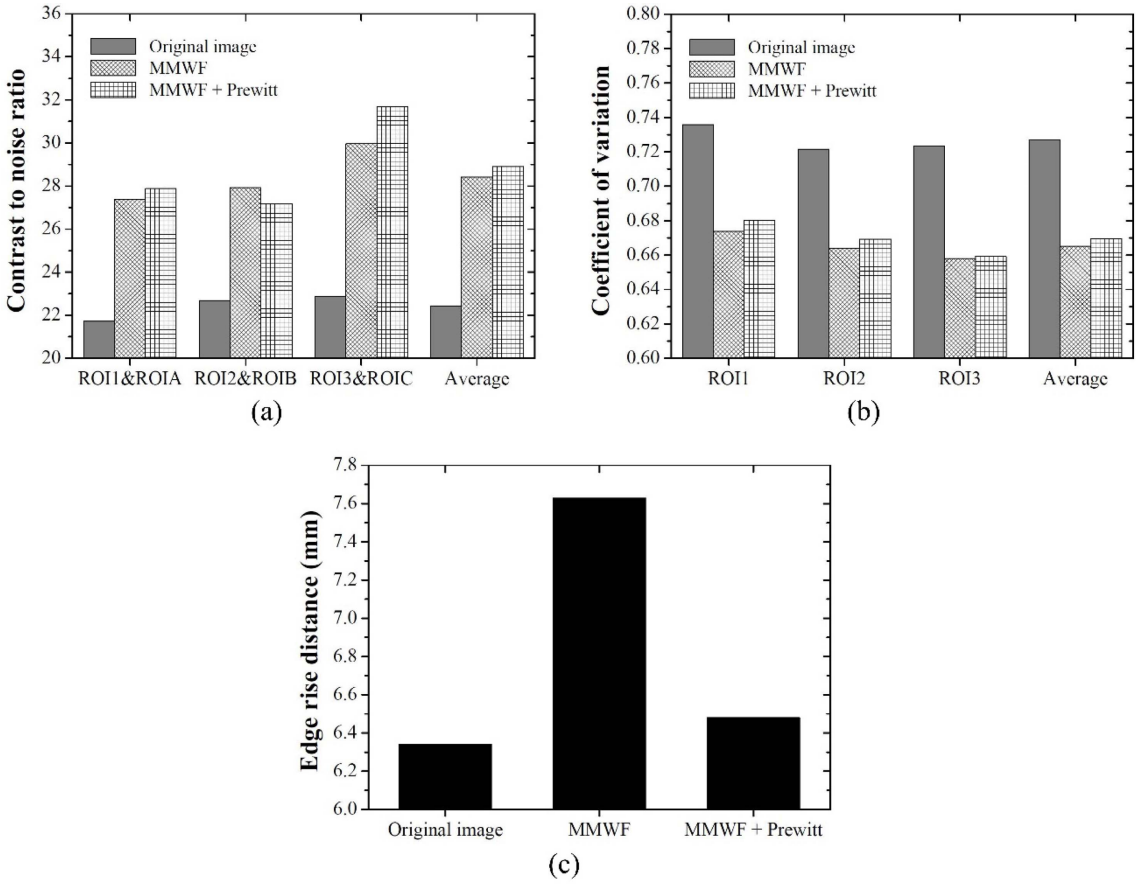

Fig. 6. Graph of quantitative evaluation results: (a) contrast-to-noise ratio (CNR), (b) coefficient of variation (COV), and (c) edge rise distance (ERD). The proposed fusion algorithm derived the superb CNR, and COV and ERD were obtained with data that could obtain appropriate noise level and edge preservation.

compared to the original image and MMWF, respectively.

These quantitative evaluation results indicate that the Prewitt operator compensated for the disadvantage of deteriorating edge information when applying MMWF. Compared to filtering methods that only remove noise, the proposed algorithm preserves edge information much better and can similarly reduce the noise level; therefore, we expect that it can be applied to a variety of medical images. In addition, we believe that the improved CNR compared with MMWF can be useful in situations where contrast and image edge areas are important when diagnosing lesions. In particular, based on the results of this study, it will be possible to improve the accuracy of segmentation and classification in various diagnostic medical images, including MR/PET images; we expect that the efficiency of artifact reduction can be increased by modeling a technology that combines the proposed algorithm and the inpainting method [26].

MMWF noise-reduction technology has been applied to various diagnostic medical images and has shown high denoising efficiency [27, 28]. Research results showing improved property evaluation results compared to wavelet technology by applying a modified MMWF to nuclear MR spectroscopy were also analyzed [27], as was the applicability of X-ray CT images [28]. The change parameter of MMWF, which has proven applicability in the field of diagnostic medical imaging, includes the mask size. The CNR and COV values vary depending on the mask size, and if the algorithm combining the Prewitt operator is optimized in the future, a more effective application to MR/PET images can be achieved.

Creating an accurate structural attenuation correction map during whole-body PET examinations is difficult. To overcome this problem, deep-learning-based PET image attenuation correction methods have been proposed [29]. Securing a dataset using a generative adversarial network (GAN) to apply deep learning technology for attenuation correction is useful. Removing noise and blurring in the preprocessing stage for applying GAN to attenuation correction of PET images is very important for improving

accuracy. Thus, we expect the algorithm proposed in this study to be used in deep learning technologies, including GAN, because it has excellent preservation of noise and edges in MR/PET images.

4. Conclusion

In this study, we proposed a method for improving the noise characteristics and edge area of attenuation-corrected MR/PET images using UTE pulse sequences. In conclusion, we demonstrated that the proposed algorithm combining MMWF and the Prewitt operator improved the quality of MR/PET images.

Acknowledgement

This study was supported by the Eulji University in 2023 and a National Research Foundation of Korea (NRF) grant funded by the Korean government (MSIT) (No. 2022R1G1A100477512).

References

[1] Y. D. Son, Y. B. Kim, J. H. Kim, J. H. Kim, D. H. Kwon, H. Lee, and Z. H. Cho, Pharmaceuticals. **15**, 583 (2022).
[2] G. M. Currie, P. Kamvosoulis, and S. Bushong, J. Nucl. Med. Technol. **49**, 217 (2021).
[3] S. Vandenberghe and P. K. Marsden, Phys. Med. Biol. **60**, R115 (2015).
[4] X. Y. Zhang, Z. L. Yang, G. M. Lu, G. F. Yang, and L. J. Zhang, Front. Mol. Neurosci. **10**, (2017).
[5] R. Cardoso and T. M. Leucker, PET Clin. **15**, 509 (2020).
[6] H. K. Ahn, H. Lee, S. G. Kim, and S. H. Hyun, Clin. Radiol. **74**, 467 (2019).
[7] H. J. Jeong, H. Lee, S. Y. Lee, S. Seo, K. H. Park, Y. B. Lee, D. J. Shin, J. M. Kang, B. K. Yeon, S. G. Kang, J. Cho, J. K. Seong, N. Okamura, V. L. Vilemagne, D. L. Na, and Y. Noh, J. Clin. Neurol. **16**, 202 (2020).
[8] C. Buchbender, V. Hartung-Knemeyer, M. Forsting, G. Antoch, and T. A. Heusner, Brit. J. Radiol. **86**, 20120570 (2012).
[9] T. Wanek, L. Schollbauer, T. Filip, S. Mairinger, M. Sauberer, M. Blaickner, and C. Kuntner, Front. Phys. **8**, (2020).
[10] W. Sureshbabu and O. Mawlawi, Proceedings. J. Nucl. Med. Technol. **33**, 156 (2005).
[11] S. L. Brady and B. L. Shulkin, Clin. Transl. Imaging. **5**, 359 (2017).
[12] Y. Chen and H. An, Magn. Reson. Imaging Clin. N. Am. **25**, 245 (2017).
[13] I. Mecheter, L. Alic, M. Abbod, A. Amira, and J. Ji, J. Digit. Imaging. **33**, 1224 (2020).
[14] M. D. Robson, P. D. Gatehouse, M. Bydder, and G. M. Bydder, J. Comput. Assist. Tomogr. **27**, 825 (2003).
[15] G. Wagenknecht, H. J. Kaiser, F. M. Mottaghy, and H. Herzog, MAGMA. **26**, 99 (2013).
[16] V. Keereman, Y. Fierens, T. Broux, Y. D. Deene, M. Lonneus, and S. Vandenberghe, J. Nucl. Med. **51**, 812 (2010).
[17] C. R. Park, S. H. Kang, and Y. Lee, Nucl. Eng. Technol. **52**, 2328 (2020).
[18] A. Le Pogam, H. HAnzouli, M. Hatt, C. Cheze Le Rest, and D. Visvikis, Med. Image Anal. **17**, 877 (2013).
[19] H. Arabi and H. Zaidi, Ann. Nucl. Med. **35**, 176 (2021).
[20] Y. Lee, Optik. **245**, 167681 (2021).
[21] R. Barik, S. Modak, M. N. B. J. Naskar, and U. Verma, Int. J. Eng. Res. Technol. **9**, 143 (2021).
[22] C. V. Cannistraci, F. M. Montevecchi, and M. Alessio, Proteomics. **9**, 4908 (2009).
[23] H. Ye, B. Shen, and S. Yan, IEEE 3rd Advanced Information Technology, Electronic and Automation Control Conference (IAEAC), (2020).
[24] M. Song, M. Kim, J. Lim, D. Chun, M. Park, J. Shim, and Y. Lee, J. Magn. **28**, 56 (2023).
[25] J. Y. Park and S. Kim, International Journal of Radiation Research **20**, 425 (2022).
[26] Q. Wang, Y. Chen, N. Zhang, and Y. Gu, Measurement. **185**, 110027 (2021).
[27] C. V. Cannistraci, A. Abbas, and X. Gao, Sci. Rep. **5**, (2015).
[28] S. Ju, S. H. Kang, and Y. Lee, Nucl. Instrum. Methods Phys. Res. Section A **1010**, 165508 (2021).
[29] X. Dong, Y. Lei, T. Wang, K. Higgins, T. Liu, W. J. Curran, H. Mao, J. A. Nye, and X. Yang, Phys. Med. Biol. **65**, 055011 (2020).